NASA TECHNICAL NOTE

NASA TN D-2355

NASA TN D-2355

RADIANCE OF THE EARTH AND ITS LIMB IN THE MIDDLE ULTRAVIOLET

by William C. Hrasky and Thomas B. McKee

Langley Research Center
Langley Station, Hampton, Va.

NATIONAL AERONAUTICS AND SPACE ADMINISTRATION • WASHINGTON, D. C. • JULY 1964

RADIANCE OF THE EARTH AND ITS LIMB IN THE MIDDLE ULTRAVIOLET

By William C. Hrasky and Thomas B. McKee

Langley Research Center
Langley Station, Hampton, Va.

NATIONAL AERONAUTICS AND SPACE ADMINISTRATION

For sale by the Office of Technical Services, Department of Commerce,
Washington, D.C. 20230 -- Price $1.00

RADIANCE OF THE EARTH AND ITS LIMB IN THE MIDDLE ULTRAVIOLET

By William C. Hrasky and Thomas B. McKee
Langley Research Center

SUMMARY

The equation for the calculated radiance in the middle ultraviolet region (0.20μ to 0.30μ) emerging from the top of a 200-kilometer-thick spherical atmosphere is derived from the geometry and physics of Rayleigh scattering and ozone absorption. The radiance is that which would be seen by a hypothetical observer 400 kilometers above the earth. The radiance is calculated for various wavelengths and sun orientations for planar scans across the earth's disk. The various atmospheric phenomena affecting the results are shown and discussed.

INTRODUCTION

Many attempts have been made to calculate expected values of the earth's radiance due to scattered solar radiation. Coulson (ref. 1) has given a definitive treatment of the expected radiance emerging from a plane-parallel atmosphere due to multiple scattering. This method is based on the theoretical treatment derived by Chandrasekhar (ref. 2). Coulson, Dave, and Sekera (ref. 3) have published tables giving the normalized radiance due to scattering for various optical depths again for a plane-parallel atmosphere.

When absorption is included, the problem is modified. Green (ref. 4) has specifically investigated the middle ultraviolet radiance ($2000\ \text{Å}$ to $3000\ \text{Å}$) due to primary scattering and ozone absorption in a plane-parallel atmosphere.

These studies were for plane-parallel atmospheres and therefore apply only approximately to the curved atmosphere of the earth; they do not apply at all to the problem of determining the brightness due to scattering at the limb as seen from a spacecraft.

The present paper gives an analysis of the radiation scattered from a curved atmosphere for the special condition in which the radiation is so strongly absorbed by the atmosphere that only the primary scattering is significant. The atmosphere used was ideally clear and composed only of molecules. The incident solar radiation was presumed to be unpolarized. Polarization of scattered light was not included in the calculations. The specific application of this

study is to the scattering of the middle ultraviolet and is thus related to the study of reference 4 for a plane-parallel atmosphere.

The appropriate equations are derived and discussed, and solutions are presented for various solar-spatial configurations. This report investigates the physical phenomena causing changes in the various scans. Comparisons with Green are shown for similar conditions.

SYMBOLS

d	length of a line, arbitrary units
e	base of Naperian logarithms
H_λ	solar spectral irradiance incident on atmosphere, $w/cm^2-\mu$
H'_λ	spectral irradiance incident on scattering element from attenuated solar beam, $w/cm^2-\mu$
h	altitude of observer, km
h_o	tangent altitude of a line of sight from surface of earth, km
h'	altitude of a scattering element on a line of sight, km
I	intensity emerging from a medium of thickness L, w/cm^2
I_o	intensity incident on a medium, w/cm^2
j_λ	spectral ozone absorption coefficient for base e, cm^{-1}
K	attenuation coefficient, inverse units of L
k_λ	spectral Rayleigh scattering coefficient for base e, km^{-1}
L	optical thickness of radiation path in a medium, arbitrary units
M	scattering optical thickness encountered on path into atmosphere, km
M'	scattering optical thickness encountered on path out of atmosphere, km
m	scattering optical thickness of scattering element, km
N	number density of atmosphere, molecules/cm^3
N_λ	spectral radiance emerging from atmosphere along a line of sight, w/cm^2-steradian-μ
N'_λ	spectral radiance emerging from atmosphere due to a scattering element, w/cm^2-steradian-μ

N''_λ	spectral radiance emerging from a scattering element in direction of line of sight, w/cm^2-steradian-μ
n	index of refraction
Q	total "effective mass" along a path, g/km^2
$p(\cos \psi)$	scattering phase function which determines angle dependence of scattering
R	radius of the earth, 6,375 km
s	length along a path, arbitrary units
T	optical thickness at an altitude, km
v	altitude of a point along a path, km
x,y,z	rectangular Cartesian coordinates, arbitrary units
α	angle made with a local vertical by a path at altitude h', deg
β	angle between a local vertical and the variable altitude line v, deg
$\Delta h'$	elemental increment of altitude along line of sight, km
θ	zenith angle of a line of sight at observer (fig. 2), deg
θ'	zenith angle of line of sight at scattering element m (fig. 2), deg
θ_o	zenith angle of sun at observer (fig. 2), deg
θ'_o	zenith angle of sun at a scattering element (fig. 2), deg
λ	wavelength, microns (or μ)
ρ	effective density, g/km^3
ρ_o	atmosphere density at sea level, g/km^3
ρ_n	depolarization factor
τ	ozone density at NTP, cm/km
ϕ	east-of-north azimuth of line of sight (fig. 3), deg
ϕ_o	east-of-north azimuth of sun (fig. 2), deg
ψ	scattering angle (fig. 2), deg
ω	absorption optical thickness of ozone encountered by incoming radiation, cm

ω' absorption optical thickness of ozone encountered by outgoing radiation, cm

Subscripts:

i any integer

1,2 refer to lines 1 and 2 in figures 3 and 4

GEOMETRY OF THE PROBLEM

A scan is defined as one sweep of an observer's line of sight across the planet in a plane (fig. 1). For purposes of clarity in discussing a scan, it is assumed that the scan begins at the southern limb and terminates at the northern limb. Actually, the geometry is such that a north-south plane is not necessary.

In this section, the basic geometric parameters to account for the spherical atmosphere are derived. These parameters are the tangent altitude of a line of sight, the scattering angle at a scattering element, and the zenith angle of the sun.

Tangent Altitude

Each scan is composed of many lines of sight defined by θ, the zenith angle of the line of sight at the observer. Figure 2 shows the geometry of one line of sight.

Here $\overline{PDBC}$ is a line of sight with the observer at point P. Point A is the center of the earth; therefore, line $\overline{AP}$ is the local vertical at P. On every line of sight there exists a point B such that the angle ABP is a right angle. The altitude of this point is h_o. By inspection of triangle ABP it is seen that

$$\sin \theta = \frac{R + h_o}{R + h} \tag{1}$$

and

$$h_o = (R + h)\sin \theta - R \tag{2}$$

where h is the altitude of the observer and R is the radius of the earth.

Scattering Angle

If a line of any orientation $\overline{EF}$ intersects the line of sight at some point D, the angle ψ is the change of direction of $\overline{EF}$ at D to line $\overline{DP}$. Line direction is indicated by arrows in figure 2. If $\overline{PE'}$ is drawn through

point P and parallel to $\overline{DE}$, it will intersect the line of sight at the same angle, ψ. Line $\overline{PE'}$ can now be assigned a zenith angle θ_o and an azimuth ϕ_o.

The line of sight has a zenith angle of θ and an azimuth of ϕ. (See fig. 3.) Since the azimuth and zenith angle of both lines are known, the angle between the line of sight and $\overline{PE'}$ can be found. From analytic geometry it is known that

$$\cos(180^\circ - \psi) = -\cos\psi = \frac{x_1x_2 + y_1y_2 + z_1z_2}{d_1d_2} \tag{3}$$

By referring to figure 3, it can be seen that

$$\left.\begin{aligned} x_1 &= -\sin\theta_o \cos(\phi_o - 90^\circ) \\ y_1 &= \sin\theta_o \sin(\phi_o - 90^\circ) \\ z_1 &= \cos\theta_o \\ |d_1| &= 1 \end{aligned}\right\} \tag{4}$$

$$\left.\begin{aligned} x_2 &= -\sin\theta \sin\phi \\ y_2 &= -\sin\theta \cos\phi \\ z_2 &= \cos\theta \\ |d_2| &= 1 \end{aligned}\right\} \tag{5}$$

If equations (4) and (5) are substituted into equation (3), the resulting equation is

$$\cos\psi = -\sin\theta_o \sin\phi_o \sin\theta \sin\phi - \sin\theta_o \cos\phi_o \sin\theta \cos\phi - \cos\theta_o \cos\theta \tag{6}$$

By moving the lines into various quadrants, it is seen that equation (6) holds for all quadrants.

Solar Zenith Angle

From figure 2 it can be seen that the line $\overline{AD}$ is the local vertical of point D. The line $\overline{DE}$ makes an angle θ_o' with $\overline{AD}$. To find a relationship for θ_o', it is necessary to refer to figure 4.

In figure 4(a), if it is assumed that the Y-axis is the line of sight, point P is on the line of sight $\overline{PC}$, $\overline{PA}$ is the local vertical, and $\overline{PE'}$ is the line parallel to $\overline{DE}$ (defined in fig. 2), then

$$\cos(180^\circ - \theta_o) = \frac{x(R + h)\sin\theta + y(R + h)\cos\theta}{R + h} \tag{7}$$

and

$$\cos\theta_o = -x\sin\theta - y\cos\theta \tag{8}$$

In figure 4(b), if it is assumed that the same coordinate system and lines $\overline{AD}$ and $\overline{DE}$ are as defined in figure 2, it is seen that

$$\cos(180^\circ - \theta_o') = \frac{x(R + h')\sin\theta' + y(R + h')\cos\theta'}{R + h'} \tag{9}$$

and

$$\cos\theta_o' = -x\sin\theta' - y\cos\theta' \tag{10}$$

By referring to figure 2 and triangle APD, it is found that

$$\sin\theta' = \left(\frac{R + h}{R + h'}\right)\sin\theta \tag{11}$$

In figure 4(c), if it is assumed that the same coordinate system is used as in figure 4(b), it is seen that

$$\cos\psi = \frac{(0)x + (1)y + (0)z}{1 \times 1} = y \tag{12}$$

Substitution of equation (12) into equation (8) gives

$$\cos\theta_o = -x\sin\theta - \cos\psi\cos\theta \tag{13}$$

The equation for x obtained from equation (13) is

$$x = -\frac{\cos\theta_o + \cos\psi\cos\theta}{\sin\theta} \tag{14}$$

If equations (14) and (12) are substituted into equation (10), the resulting equation is

$$\cos\theta_o' = \frac{\cos\theta_o\sin\theta' + \cos\psi\cos\theta\sin\theta'}{\sin\theta} - \cos\psi\cos\theta' \tag{15}$$

There are now three variables of the geometry determined: h_o, ψ, and θ_o'. What is more important, all are related to one variable, the zenith angle θ.

SCATTERING AND ABSORPTION

Rayleigh scattering holds to Beer's law. The absorption problem was investigated and the assumption was made that the absorption in this study held to Beer's law, also. According to Beer's law, if a beam of intensity I_o passes through a medium of path length L and an attenuation coefficient K, the intensity of the beam emerging from the medium is I, where from reference 5 and in the notation of the present paper

$$I = I_o e^{-KL} \tag{16}$$

Attenuation is the diminishing of the beam intensity by the medium; it may be due to absorption alone or to both absorption and scattering. If attenuation is due to both absorption and scattering,

$$K = k_\lambda + j_\lambda \tag{17}$$

where k_λ is the scattering coefficient and j_λ is the absorption coefficient. In this problem, k_λ is the Rayleigh scattering coefficient defined by (ref. 6)

$$k_\lambda = \frac{32\pi^3(n - 1)^2}{3\lambda^4 N}\left(\frac{6 + 3\rho_n}{6 - 7\rho_n}\right) \times 10^5 \tag{18}$$

and j_λ is the ozone absorption coefficient.

Figure 2 shows the path of the radiation within the geometry of the problem. The parallel incident solar radiation enters the atmosphere and is attenuated on its way to the scattering element on the line of sight by the scattering optical thickness M and the absorption optical thickness ω of the atmosphere. Some of the radiation scattered by the scattering optical thickness of the scattering element m out of the incident beam has the direction of the line of sight. The scattered radiation is further attenuated by the outgoing scattering optical thickness M' and the outgoing absorption optical thickness ω' until it emerges from the top of the atmosphere.

The optical thicknesses, along with the physics of scattering at the scattering element, and the ultimate emerging radiance are now examined.

Optical Thicknesses

It is important to know how to determine these optical thicknesses, M, M', ω, and ω'. From figure 5 it is seen that these are the key values in applying the problem to a spherical atmosphere.

Figure 5 shows an arbitrary path $\overline{ED}$ in the atmosphere down to a certain altitude h'. The path makes an angle α with the local vertical. It is necessary to find the total "effective attenuation mass" along this path. The general problem is treated in reference 7. If Q is the effective mass per unit area, then along the path $\overline{ED}$

$$Q = \int_{\overline{ED}} \rho \, ds \tag{19}$$

where ρ is density at ds. Since ρ is a function of altitude v, then by changing variables it is seen that

$$Q = \int_{h'}^{200} \frac{\rho(v)dv}{\cos \beta} = \int_{h'}^{200} \frac{\rho(v)dv}{\sqrt{1 - \sin^2\beta}} \tag{20}$$

where the effective upper altitude was found to be 200 kilometers. From triangle DCA in figure 5, it can be seen that

$$\sin \beta = \left(\frac{R + h'}{R + v}\right) \sin \alpha \tag{21}$$

If equation (21) is substituted into equation (20), the resulting equation is

$$Q = \int_{h'}^{200} \frac{\rho(v)dv}{\sqrt{1 - \left(\frac{R + h'}{R + v}\right)^2 \sin^2\alpha}} \tag{22}$$

However, Q is the effective mass, not the optical thickness. If optical thickness T is defined as that length of path which would be traversed at sea level at normal temperature and pressure (NTP) and have the same effective mass, than equation (22) becomes

$$T = \frac{Q}{\rho_o} = \frac{1}{\rho_o} \int_{h'}^{200} \frac{\rho(v)dv}{\sqrt{1 - \left(\frac{R + h'}{R + v}\right)^2 \sin^2\alpha}} \tag{23}$$

where ρ_o is the density at sea level. It can be seen by comparing figures 2 and 5 that the angle α is either θ' or θ_o', depending on whether path $\overline{DP}$ or path $\overline{ED}$ is used.

If M is the scattering optical thickness of the incoming path, as seen in figure 2, which makes an angle of θ_o' with the local vertical of m, then

$$M = \frac{1}{\rho_o} \int_{h'}^{200} \frac{\rho(v)dv}{\sqrt{1 - \left(\frac{R + h'}{R + v}\right)^2 \sin^2\theta_o'}} \tag{24}$$

In this study $\rho(v)$ values are taken from reference 8.

For ω, the values of the ozone concentration $\tau(v)$ are taken from reference 9. These values are in absorption optical thickness per altitude change at a particular altitude (cm/km). Therefore, ω has the form

$$\omega = \int_{h'}^{200} \frac{\tau(v)dv}{\sqrt{1 - \left(\frac{R + h'}{R + v}\right)^2 \sin^2\theta_o'}} \tag{25}$$

The scattering element lies along the line of sight, as in figure 2. For any scattering element on the line of sight, it is seen that

$$m = \frac{1}{\rho_o} \int_{h'}^{h'+\Delta h'} \frac{\rho(v)dv}{\sqrt{1 - \left(\frac{R + h'}{R + v}\right)^2 \sin^2\theta'}} \tag{26}$$

If triangle ADB in figure 2 is examined and the law of sines is used, the resulting equation is

$$(R + h')\sin\theta' = R + h_o \tag{27}$$

Squaring equation (27) and substituting the result into equation (26) gives

$$m = \frac{1}{\rho_o} \int_{h'}^{h'+\Delta h'} \frac{\rho(v)dv}{\sqrt{1 - \left(\frac{R + h_o}{R + v}\right)^2}} \tag{28}$$

Since both M' and ω' lie along the line of sight, then

$$M' = \frac{1}{\rho_o} \int_{h'+\Delta h'}^{200} \frac{\rho(v)dv}{\sqrt{1 - \left(\frac{R + h_o}{R + v}\right)^2}} \tag{29}$$

and

$$\omega' = \int_{h'+\Delta h'}^{200} \frac{\tau(v)dv}{\sqrt{1 - \left(\frac{R + h_o}{R + v}\right)^2}} \tag{30}$$

By looking at figure 2 it is seen that equations (29) and (30) are correct only if m lies between points B and P. If m lies on the other side of B, ω' equals the integration from m to point B and then from B to 200 kilometers - that is,

$$M' = \frac{1}{\rho_o}\left[\int_{h_o}^{h'-\Delta h'} \frac{\rho(v)dv}{\sqrt{1 - \left(\frac{R + h_o}{R + v}\right)^2}} + \int_{h_o}^{200} \frac{\rho(v)dv}{\sqrt{1 - \left(\frac{R + h_o}{R + v}\right)^2}}\right] \tag{31}$$

and

$$\omega' = \int_{h_o}^{h'-\Delta h'} \frac{\tau(v)dv}{\sqrt{1 - \left(\frac{R + h_o}{R + v}\right)^2}} + \int_{h_o}^{200} \frac{\tau(v)dv}{\sqrt{1 - \left(\frac{R + h_o}{R + v}\right)^2}} \tag{32}$$

Emerging Radiance

The problem now is to travel the path of the radiation and analytically formulate the radiance equation as the path is traversed. Beer's law (eq. 16)) defines the spectral irradiance incident on m after attenuation of the incident solar beam by scattering and absorption as

$$H_\lambda' = H_\lambda e^{-\left(k_\lambda M + j_\lambda \omega\right)} \tag{33}$$

where H_λ is the solar spectral irradiance at the top of the atmosphere.

Radiation is scattered out of the incident beam by m. The fraction of the incident radiation scattered by m is $k_\lambda m$.

According to Chandrasekhar (ref. 2), the distribution of Rayleigh scattered light follows a phase function

$$p(\cos \psi) = \frac{3}{4}\left(1 + \cos^2\psi\right) \tag{34}$$

The angle ψ is the scattering angle defined by equation (6). The coefficient 3/4 is a normalizing factor such that if the phase function is integrated over 4π steradians, the result will be unity.

It can now be said that the spectral radiance N_λ'' emerging from m along the line of sight toward point P is

$$N_\lambda'' = \frac{3}{4}\left(1 + \cos^2\psi\right)\frac{1}{4\pi} k_\lambda m H_\lambda e^{-\left(k_\lambda m + j_\lambda \omega\right)} \tag{35}$$

As this radiation travels from m to the top of the atmosphere along the line of sight, it is again attenuated by scattering and absorption. Therefore, the spectral radiance, N_λ' emerging from the top of the atmosphere due to m is

$$N_\lambda' = \frac{3}{4}\left(1 + \cos^2\psi\right)\frac{1}{4\pi} k_\lambda m H_\lambda e^{-k_\lambda(M+M') - j_\lambda(\omega+\omega')} \tag{36}$$

If the contributions from each m_i along the line of sight are summed, the total spectral radiance N_λ is

$$N_\lambda = \frac{3}{4}\left(1 + \cos^2\psi\right)\frac{1}{4\pi} H_\lambda k_\lambda \sum_i m_i e^{-k_\lambda\left(M_i + M_i'\right) - j_\lambda\left(\omega_i + \omega_i'\right)} \tag{37}$$

Equation (37) is the fundamental equation of this calculation. This expression was evaluated on the IBM 7090 electronic data processing system.

CALCULATED RESULTS

The program characteristics are discussed in this section. The typical scan has been separated into the nadir and the limb for discussion purposes. The contributions from various segments of the atmosphere to the emerging radiance are also investigated.

Machine Inputs

In the machine solution of equation (37) the 1959 ARDC model atmosphere was used; this atmosphere was terminated at 200 kilometers. The $\Delta h'$ used was 4 kilometers. The integrations were carried out by use of a Gaussian approximation.

The scattering and absorption coefficients used are shown as a function of wavelength in figure 6. These coefficients were taken from reference 9. According to this reference (pages 16-21) the ozone absorption coefficients were determined by Inn and Tanaka. The scattering coefficients were determined by using equation (18). The scattering curve shows the typical Rayleigh shape which is approximately proportional to λ^{-4}. The ozone absorption curve shows its peak at 0.255μ. The curve is fairly symmetrical about the peak.

The ozone distributions used to calculate ω and ω' were taken from reference 9 and are shown in figure 7. Curve A was a measured distribution taken at latitude 18°31' N. Curve B was also measured and was taken at latitude 69°40' N. For both distributions the ozone concentration was negligible above 80 kilometers. Also included in the figure for comparison is a distribution used by Green (ref. 4).

The solar spectral irradiance used as the initial radiation input to the calculation was taken from reference 9. These values are presented in the faired curve in figure 8.

The extension of the computer program to the near ultraviolet and visible regions is risky without adding the phenomena of multiple scattering and earth reflections to the calculations. Any wavelength which can penetrate to the earth's surface and which is shorter than about 0.6μ must have multiple scattering and earth reflections included. The region within the first 10 kilometers above the earth is the significant multiple scattering contributor to the radiance.

Another aspect of extending the program is the problem of atmospheric refraction. Fortunately, most of the middle ultraviolet region never gets into the extremely dense portion of the atmosphere where refraction becomes important when looking tangentially to the limb (ref. 10). This is not true for the near ultraviolet or visible region which does penetrate below 15 kilometers.

Nadir of the Scan

The nadir part of any scan ($\theta = 0°$) is especially interesting because the outgoing optical thickness can be held constant while all the other parameters are varied. Plotted in figure 9 are the nadir radiance values for each wavelength with various ozone distributions and solar positions.

Green's "standard" ozone distribution (ref. 4) with the sun at the zenith is also included in figure 9. The curves with the same sun position and different ozone curves show the effect of ozone distribution. Also shown are the measurements made in this region by Hennes (ref. 11) and those reported in reference 12. Green used an empirical expression to represent his ozone distribution. He then carried the ozone right to the top of his atmosphere. As stated previously, the ozone distributions used herein were insignificant above 80 kilometers. The difference in these two approaches can be seen in figure 9. Since there was more ozone in distributions A and B above 30 kilometers (fig. 7), the curves of figure 9 fell below Green's "standard" in the region of high absorption. The reason for the increase over Green's curve at wavelengths greater than 0.28μ is that below 20 kilometers Green's distribution had more ozone, as seen in figure 7, and therefore less radiation was scattered out of this region in Green's distribution.

The change in the position of the sun ($\theta_o = 45°$, $\phi_o = 180°$) caused a drop in nadir radiance at all wavelengths as seen in figure 9. This drop was the

result of increasing the optical thickness within the atmosphere through which the incident solar radiation had to pass before being scattered and of decreasing the magnitude of the phase function. Since the optical thickness was lengthened, more ozone was encountered and more absorption occurred. When the sun was at the zenith, the factor $1 + \cos^2\psi$ was 2.0. When the zenith angle of the sun increased to 45°, the factor $1 + \cos^2\psi$ became 1.5. The change in the scattering angle alone resulted in a 25-percent decrease in nadir radiance.

In figure 10 the spectral radiance for a scan of 0.26μ is shown as a function of zenith angle of the look line from the observer. The values of the factor $1 + \cos^2\psi$ are also presented as a function of zenith angle in this figure. The factor $1 + \cos^2\psi$ is then divided out of the radiance curve to obtain the curve identified by the dash-dot line. The minimum value for the 0.26μ scan $(\theta_o = 45^\circ, \ \phi_o = 180^\circ)$ occurred at a zenith angle of 35° S. After removing the ψ-effect, the minimum value returned to the 0° zenith-angle position in all calculations performed it was found that the position of the minimum radiance value of a scan curve was influenced by the minimum value of the factor $1 + \cos^2\psi$.

The Limb

Another point to be made after studying the scan curve (fig. 10) is that the northern maximum value is larger than the southern value. This effect is again due entirely to the ψ-effect. When the curve without the ψ-effect is examined, it is seen that the northern maximum value is now less than the southern value. This effect is due to the increased path the solar radiation must travel to reach the northern limb. Figure 10 indicates the strong effect of ψ on the shape of the scan curve.

The curve of $1 + \cos^2\psi$ is seen to drop to a minimum near the southern limb where the scattering angle ψ approaches 90°. Near the northern limb, ψ approaches 0° and, therefore, a maximum occurs. This effect occurs, again, only when the azimuth of the sun is other than 90° (when the azimuth of the sun is not perpendicular to the scan).

The peak or the maximum value near the limb is caused by the interaction of two phenomena. As the line of sight enters the top of the atmosphere and begins to sweep toward the earth, the optical thickness within the atmosphere of the line of sight increases, and the density of the atmosphere through which the line of sight is passing becomes greater. This gives more and more contributions from scattering to the emerging radiance. At the same time, the attenuation due to scattering and ozone absorption is becoming greater before and after the scattering element as the scan approaches the earth. While the line of sight is above most of the ozone and dense atmosphere, the scattering contribution is dominant and a steady rise in radiance is seen. At some tangent altitude, however, the line of sight begins to pass through more dense atmosphere with a greater concentration of ozone; the attenuation effect gains the dominance and a steady decline in radiance begins. Therefore, the peak occurs

at the altitude at which the scattering contribution is dominant, but the attenuation effect is about to become dominant.

Since both scattering and absorption are dependent on wavelength, it is not surprising that the altitude and the radiance of the peak are wavelength dependent. The peak parameters are, of course, dependent on the ozone and atmosphere density distribution, also. Figure 11 gives the peak radiances for various wavelengths, ozone distributions, and sun orientations. Figure 12 gives the peak altitudes for various wavelengths and ozone distributions.

In figure 11, it is seen that the peak radiances for the extreme sun orientation ($\theta_o = 45^o$, $\phi_o = 180^o$) are greater than that for the zenith angle $\theta_o = 0^o$. This result is due to the ψ-effect increasing the output of scattered radiation. The change in the tangent altitude at which peak radiance occurs is caused by different ozone distributions as seen in figure 12. Between wavelengths of 0.24μ and 0.26μ the radiance is not affected by the change in ozone distributions (fig. 11). This is the spectrum area where ozone absorption is the greatest. The area of less ozone absorption is definitely affected. It is evident from figure 12 that the same results found for the radiance are true for the peak altitude.

The peaks for the wavelength region between 0.24μ and 0.26μ occur above or just below the 60-kilometer altitude. The ozone-distribution curves diverge at approximately 60 kilometers. Therefore, in the extreme ozone sensitive region the radiances and altitudes of the peaks are unchanged because they occur before the two ozone distributions differ. Since the altitudes of the peaks of the less sensitive region occur lower than 60 kilometers, they are effectively altered by the change in the ozone distribution. With an increase in ozone, the peaks occur at a higher altitude and, therefore, the radiance of the peak is reduced. (See fig. 13.) The entire middle ultraviolet region has been integrated by using the ozone distribution curve A of figure 7. The scattering curves show that the peak will occur at an altitude less than 20 kilometers. With the ozone added, the peak occurs near 60 kilometers with much less radiance. It can be seen that upon the addition of more ozone above 60 kilometers, the peak would occur at a higher altitude and have a smaller radiance. Thus, it is seen that the peak radiance and its altitude are strongly dependent on the vertical distribution of ozone.

The altitude of the peaks is also effectively changed by means of sun orientation. (See fig. 14.) This change is due to the change in optical thickness of the radiation path in passing through the atmosphere. Near the southern limb, the optical thickness is smaller for the extreme sun orientation ($\theta_o = 45^o$, $\phi_o = 180^o$) than for the zenith case ($\theta_o = 0^o$). Near the northern limb, the optical thickness is greater for the extreme sun orientation than for the zenith case. These differences cause the optical thickness to become larger at a higher or lower altitude depending on which limb is being considered.

When the observer's altitude is varied, the lines of sight change with respect to the scattering angle ψ and the optical thickness. To check this effect, the peak radiances and altitudes were compared for observer altitudes

of 225, 400, and 1000 kilometers. The results showed that the change between the 225-kilometer altitude and the 1000-kilometer altitude was so small that the effect may be neglected when considering the effects of the other phenomena.

Emerging Radiance

In the previous section the change in radiance and altitude of the radiance peaks due to changes in ozone distribution brought out the interesting question of where the basic contributions to the emerging radiance take place within the atmosphere. Figure 15 shows the emerging radiance contributed from the atmosphere in segments from sea level to various altitudes. If ozone curve A (fig. 7) and 0.22μ wavelength exist for the nadir when $\theta_o = 0^o$, then figure 15 shows that the segment from 0 to approximately 30 kilometers contributes nothing to the spectral radiance. All the radiance emerging at a wavelength of 0.22μ originated between 30 and 80 kilometers. It should be remembered that the molecular oxygen absorption band has its long wavelength cut off at about 0.22μ; therefore, since O_2 absorption was not included in the calculations, the specific altitudes mentioned for 0.22μ will be higher and the radiance will be lower when this absorption is included.

If a wavelength of 0.26μ is used, then figure 15 shows that all the radiance originates in the segment of the atmosphere between approximately 40 and 90 kilometers. The increase in the altitude of the lower limit of the effective segment over that of the 0.22μ wavelength is due, of course, to the increased absorption at 0.26μ. To get a good idea of the total radiance, the measurement must be made at an altitude higher than 90 kilometers.

An estimation of the maximum error resulting from the assumption that only primary Rayleigh scattering occurs can be made by using the information in figure 15. For a wavelength of 0.22μ, the segment of the atmosphere from sea level to 30 kilometers contributes nothing to the emerging radiance. It can then be said that the effective atmosphere for this wavelength is that region of the atmosphere above 30 kilometers. If only scattering occurred in this effective atmosphere, the error due to multiple scattering when primary scattering is assumed can be found by dividing the values in column 4 by those in column 2 in table 2.1 of reference 13 (p. 40). Some of the values used were obtained from an extrapolation on the small value end of the table, since some of the calculated values fell in this region. This error is found to be a factor of 1.18. Since absorption also takes place in the effective atmosphere, the value is actually less and it can be assumed that a factor of 1.18 is the maximum error possible.

For a wavelength of 0.26μ (see fig. 15), the effective atmosphere is at a height of 40 kilometers and above. The maximum error due to multiple scattering is a factor of 1.01. This value was found as described previously for a wavelength of 0.22μ.

The emerging radiation at 0.30μ (see fig. 15), has an effective atmosphere which includes the entire atmosphere. The maximum error is found to be a factor of 3.04. For this wavelength caution must be used in evaluating the radiance values calculated.

For the limb, the peaks occur at such high altitudes that the radiation never reaches the dense atmosphere where multiple scattering is effective.

In examining figure 15, it can be seen that scattering contributes less than 1 percent to the emerging radiance above 100 kilometers regardless of the wavelength used between 0.22μ and 0.30μ. Time could have been saved by reducing the model atmosphere to 100 kilometers without sacrificing accuracy.

Plane-Parallel Atmosphere

Of interest also was the discrepancy between the results from the plane-parallel atmosphere and the spherical atmosphere, and where the discrepancy became intolerable. Figure 16 shows the spectral radiance for the spherical and plane-parallel atmospheres as a function of zenith angle for the sun at the zenith, Green's "standard" ozone distribution, and a wavelength of 0.26μ. The plane-parallel atmosphere was approximated by assuming an extremely enlarged earth in the computer program. In both calculations the altitude of the observer was held at 400 kilometers. At 60° zenith angle and 400-kilometer altitude, the error was 13.1 percent. For the spherical atmosphere the limb peak will be reached at about 71°, whereas for the plane-parallel atmosphere the limb continues its gradual climb and passes 70° toward infinity at 90°. By dropping the altitude of the observer from 400 to 200 kilometers, the zenith angle at which the error is 13 percent is approximately 63°. Therefore, the error at a given zenith angle is dependent entirely on the altitude of the observer.

CONCLUDING REMARKS

The equation for the radiance in the middle ultraviolet region emerging from the top of a 200-kilometer-thick spherical atmosphere has been derived from the geometry and the physics of Rayleigh scattering and ozone absorption. Calculations were made which exhibited the effects of various wavelengths, sun orientations, and ozone distributions on the emerging radiance of a scan of the earth's disk.

It has been shown that the scattering-angle effect is a powerful phenomenon and determines the shape of the radiance scan. This effect was even more noticeable for the limb results than for the on-earth results. Therefore, the knowledge of the sun's orientation is even more important in predicting the emerging radiance.

In the high absorption region of the middle ultraviolet it has been shown that the altitude and intensity of the limb radiance peak is extremely sensitive to the ozone distribution above 60 kilometers. This sensitivity indicates that more precise measurements of the ozone distribution in this region are necessary.

The calculations gave 60 kilometers as the tangent altitude of the peak of the emerging spectral radiance for 0.26μ. Radiations at wavelengths other than 0.26μ peaked at lower altitudes.

The density of the atmosphere above 100 kilometers was too low for Rayleigh scattering to be an effective contributor in the middle ultraviolet region. Therefore, an observer at 100 kilometers could essentially see the entire emerging radiance from the nadir.

Langley Research Center,
National Aeronautics and Space Administration,
Langley Station, Hampton, Va., March 14, 1964.

REFERENCES

1. Coulson, Kinsell, L.: The Flux of Radiation From the Top of a Rayleigh Atmosphere. Sci. Rep. No. 1 (AFCRC TN 59 402, ASTIA AD 216 317), Dept. Meteorology, Univ. of California at Los Angeles, Jan. 1959.

2. Chandrasekhar, S.: Radiative Transfer. Dover Pub., Inc., c.1960.

3. Coulson, Kinsell L., Dave, Jitendra V., and Sekera, Zdenek: Tables Related to Radiation Emerging From a Planetary Atmosphere With Rayleigh Scattering. Univ. of California Press, 1960.

4. Green, Alex E. S.: Attenuation by Ozone and the Earth's Albedo in the Middle Ultraviolet. ERR-AN-221, Space Sci. Lab., Gen. Dynamics/Astronautics, Oct. 26, 1962.

5. Deirmendjian, Diran: Attenuation of Light in the Earth's Atmosphere and Related Problems. Sci. Rep. No. 1 (Contract No. AF 19(122)-239), Dept. Meteorology, Univ. of California at Los Angeles, July 1952.

6. Penndorf, Rudolf: Tables of the Refractive Index for Standard Air and the Rayleigh Scattering Coefficients for the Spectral Region Between 0.2 and 20.0 μ and Their Application to Atmospheric Optics. Jour. Optical Soc. of America, vol. 47, no. 2, Feb. 1957, pp. 176-182.

7. Ely, John T. A.: Atmospheric Depth and Effective Solid Angle for Radiation Penetrating the Atmosphere. Geophys. Res. Papers No. 74 (AFCRL-62-260), Air Force Cambridge Res. Labs., Feb. 1962.

8. Minzner, R. A., Champion, K. S. W., and Pond, H. L.: The ARDC Model Atmosphere, 1959. Air Force Surveys in Geophysics No. 115 (AFCRC-TR-59-267), Air Force Cambridge Res. Center, Aug. 1959.

9. Anon.: Handbook of Geophysics. Revised ed., The Macmillan Co., 1961.

10. Cameron, Winifred Sawtell, Glenn, John H., Carpenter, M. Scott, and O'Keefe, John A.: The Effect of Refraction on the Setting Sun as Seen From Space in Theory and Observation. NASA TN D-1721, 1963.

11. Hennes, J. P., Fowler, W. B., and Dunkelman, L.: Middle Ultraviolet Day Radiance of the Atmosphere. Trans., American Geophys. Union (Meteorology Abstracts), vol. 43, no. 4, Dec. 1962, p. 436.

12. Friedman, R. M., Rawcliffe, R. D., and Meloy, G. E.: Radiance of the Upper Atmosphere in the Middle Ultraviolet. Rep. No. TDR-169(3260-50) TN-4 (SSD-TDR-63-162), Aerospace Corp. (El Segundo, Calif.), July 26, 1963.

13. Sobolev, V. V. (S. I. Gaposchkin, trans.): A Treatise on Radiative Transfer. D. Van Nostrand Co., Inc., c.1963.

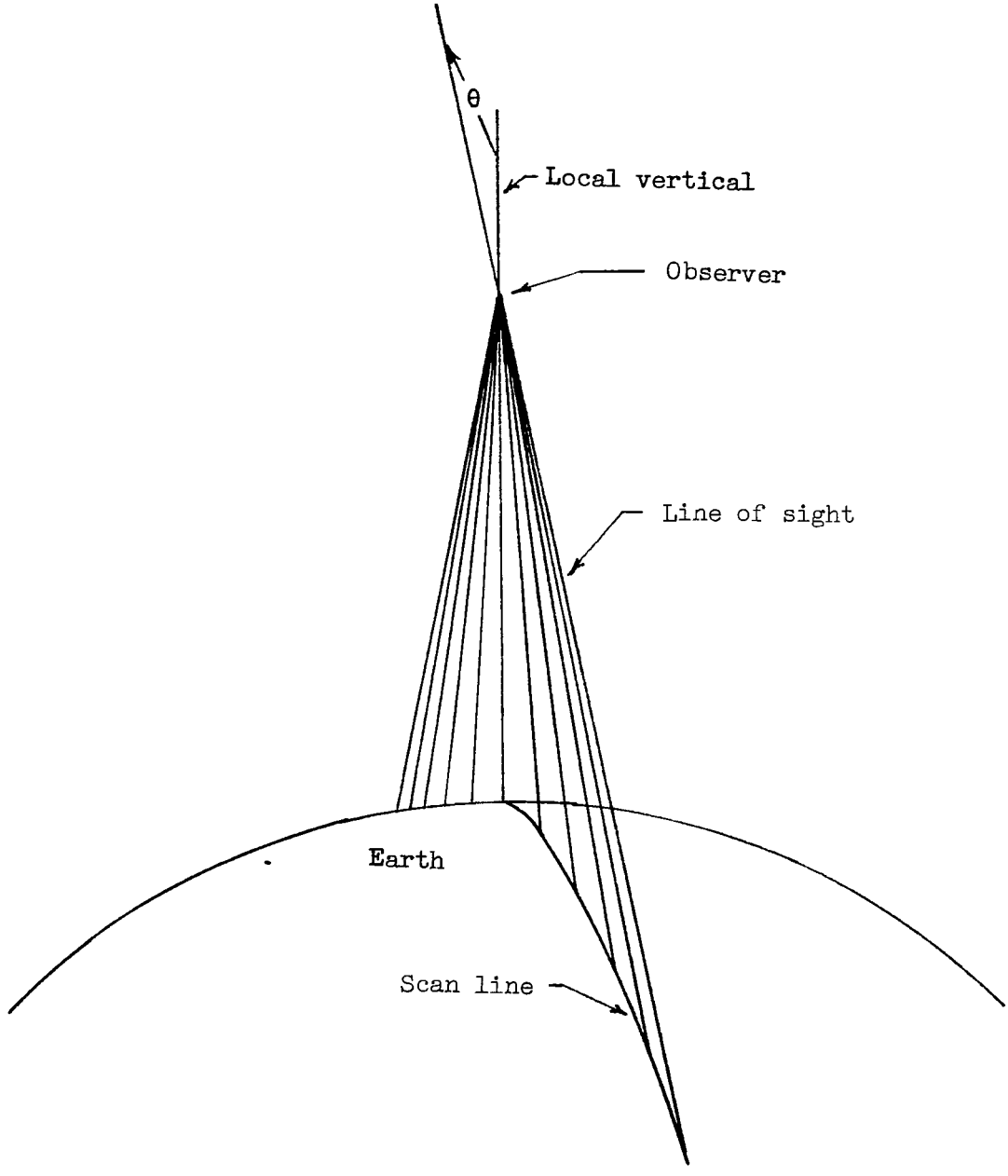

Figure 1.- The geometry of a scan.

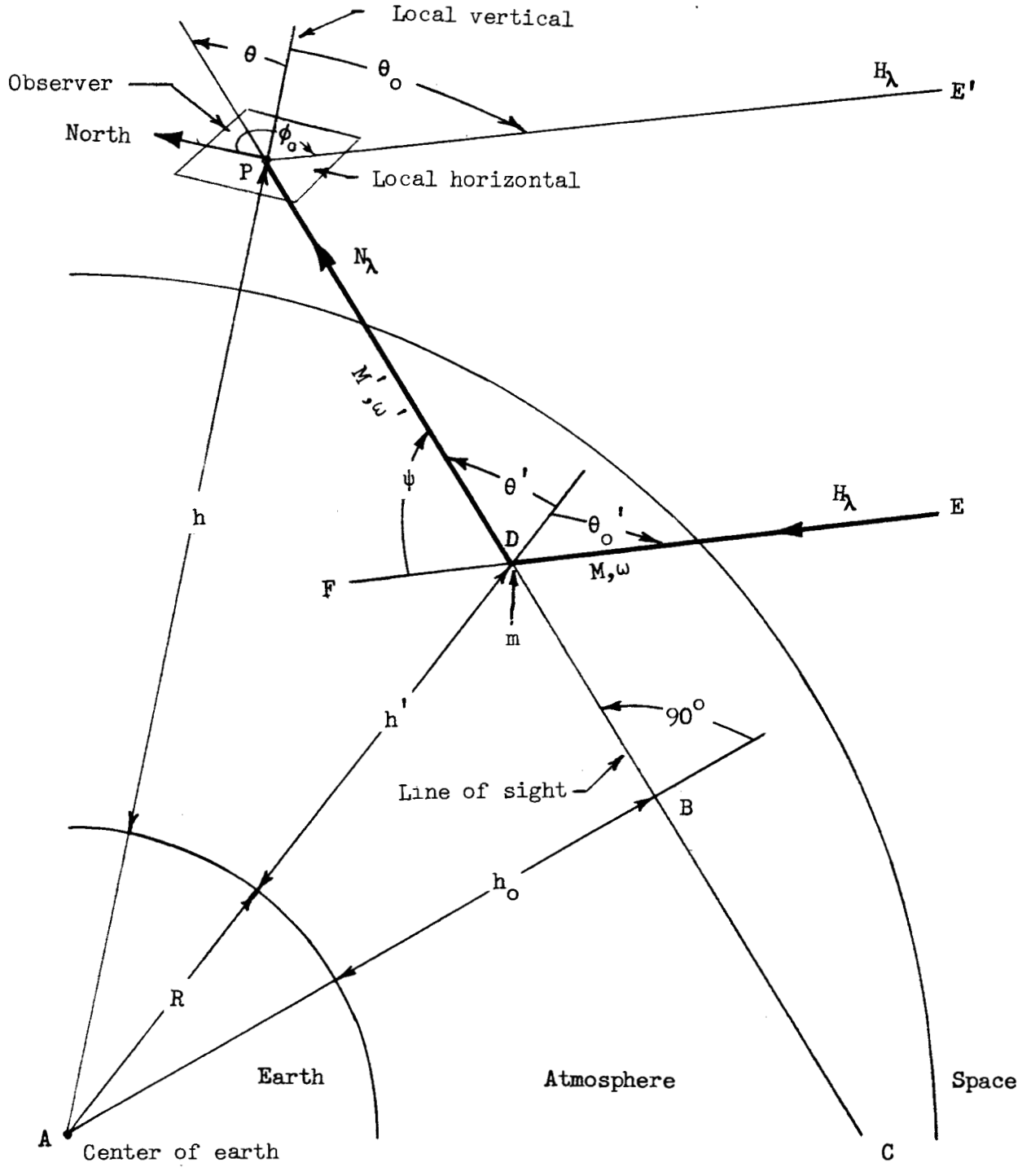

Figure 2.- The problem geometry.

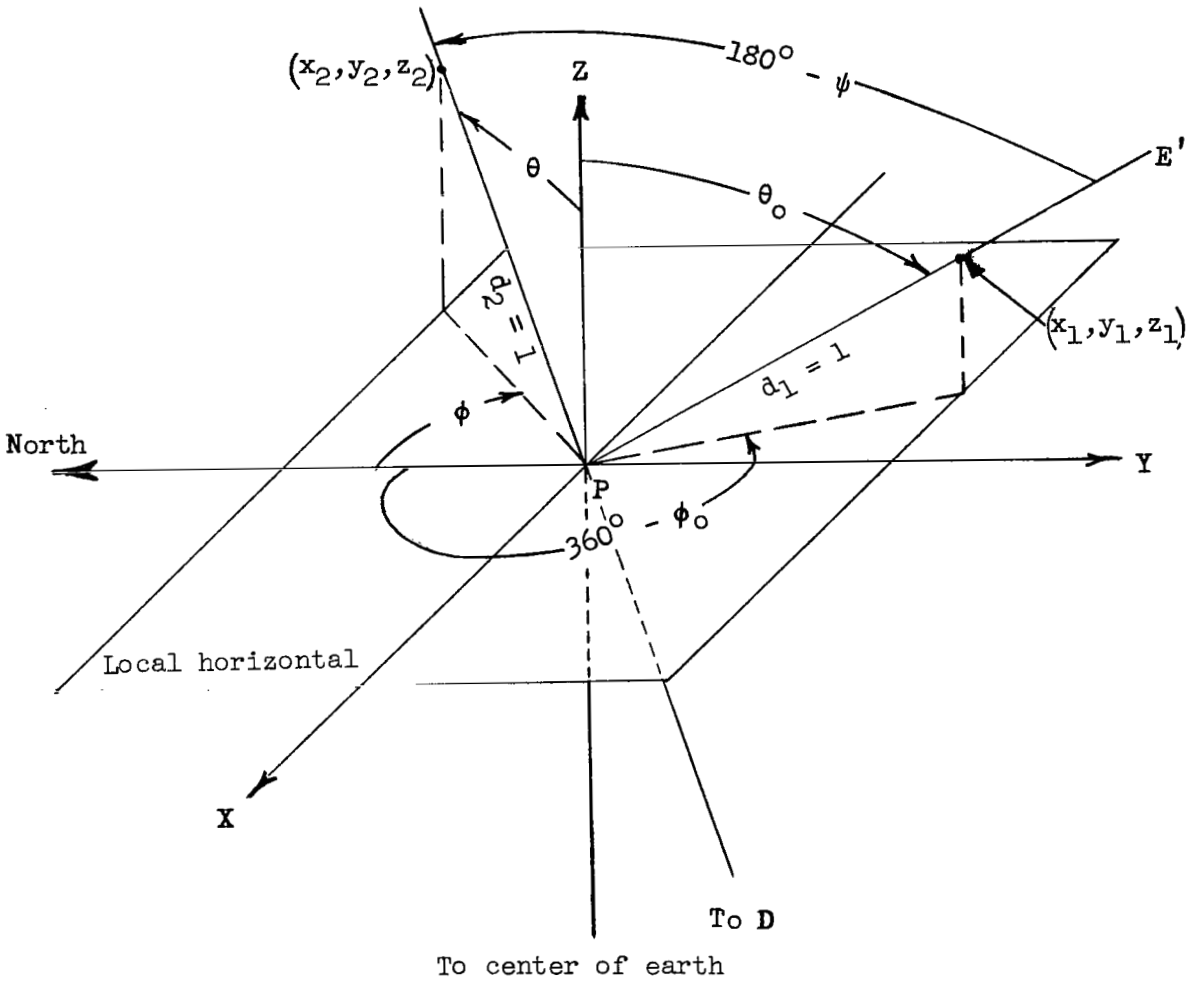

Figure 3.- The geometry at the observer.

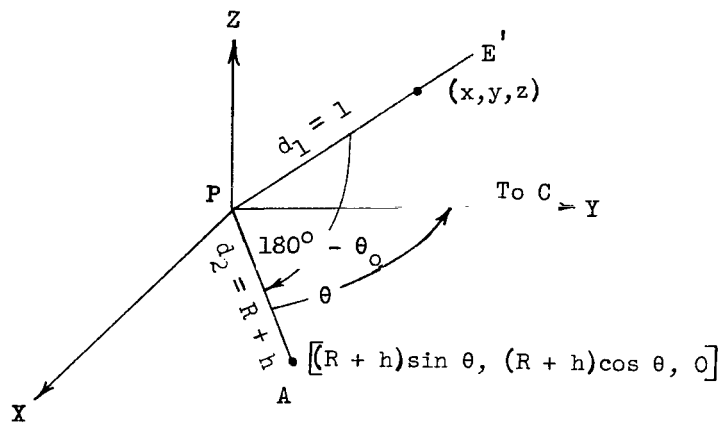

(a) Zenith angle of solar radiation at observer.

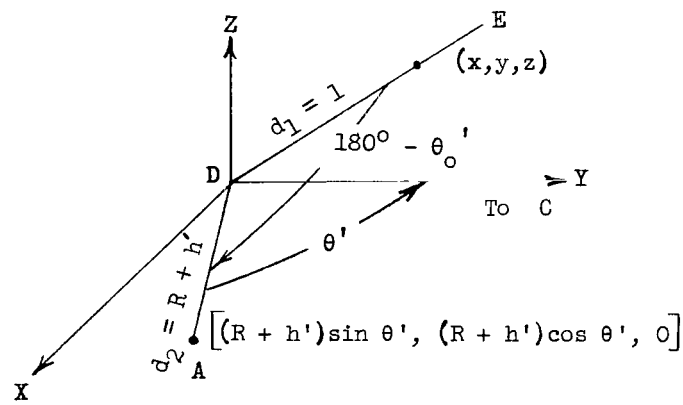

(b) Zenith angle of solar radiation at some point on line of sight.

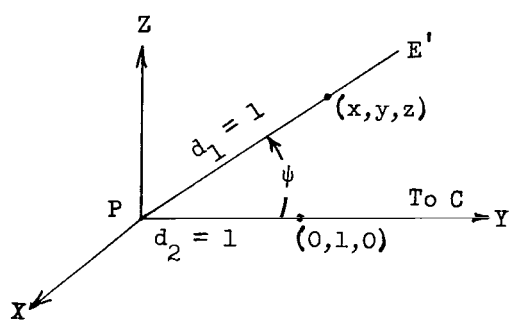

(c) Scattering angle at observer.

Figure 4.- The geometry of solar zenith angle.

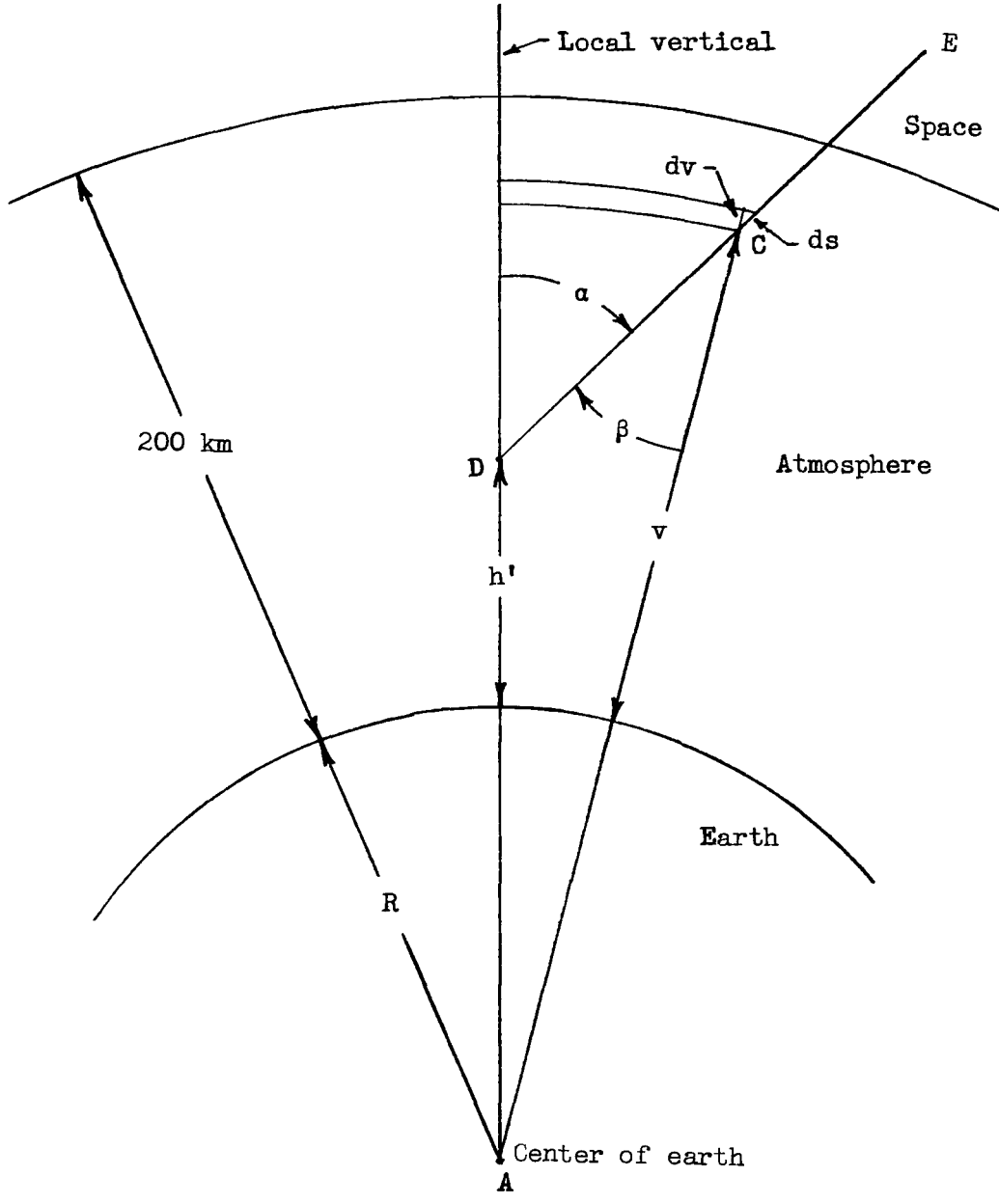

Figure 5.- Geometry of optical thickness.

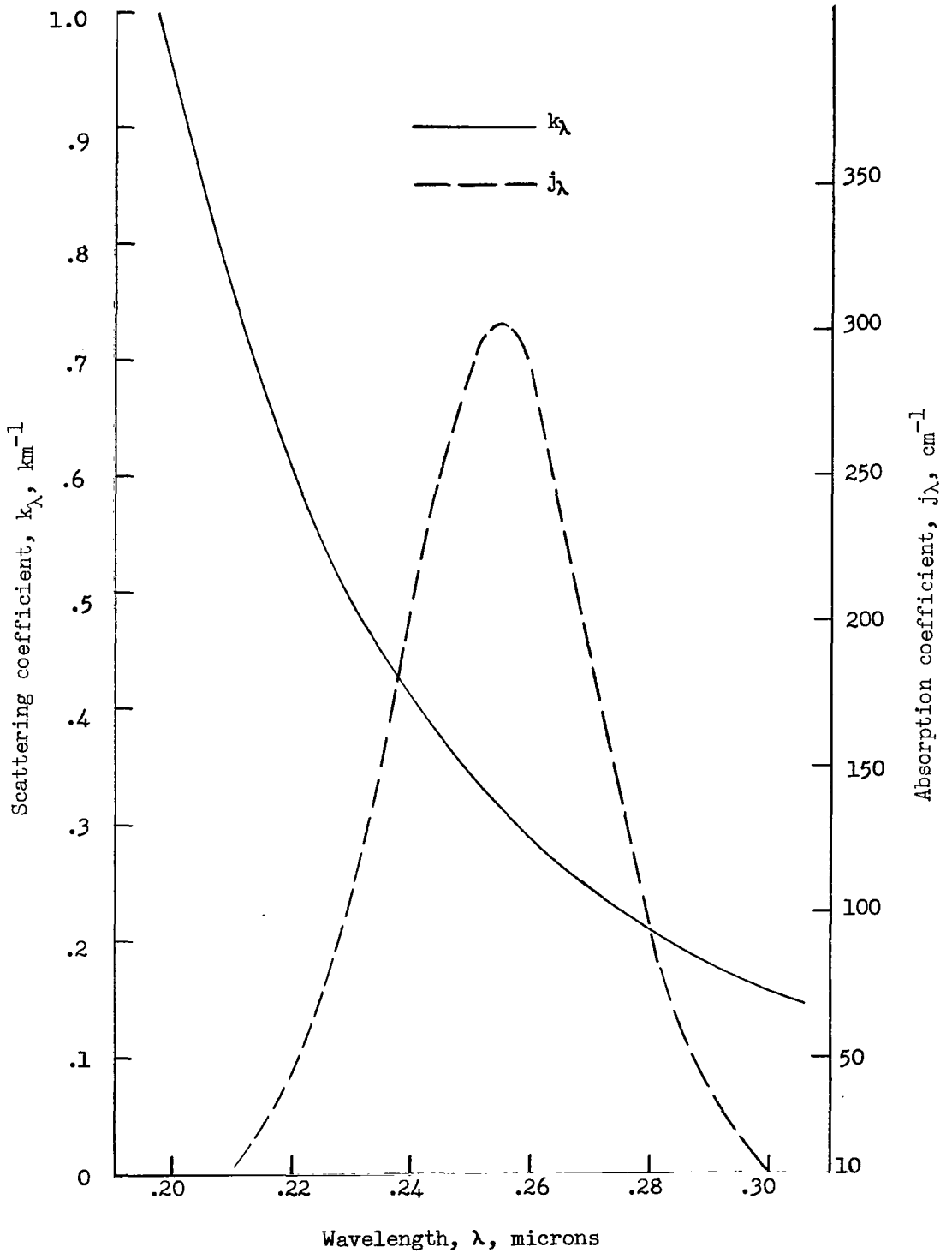

Figure 6.- Rayleigh scattering and absorption coefficients. (Data from ref. 9, tables 16-15 and 16-16A.)

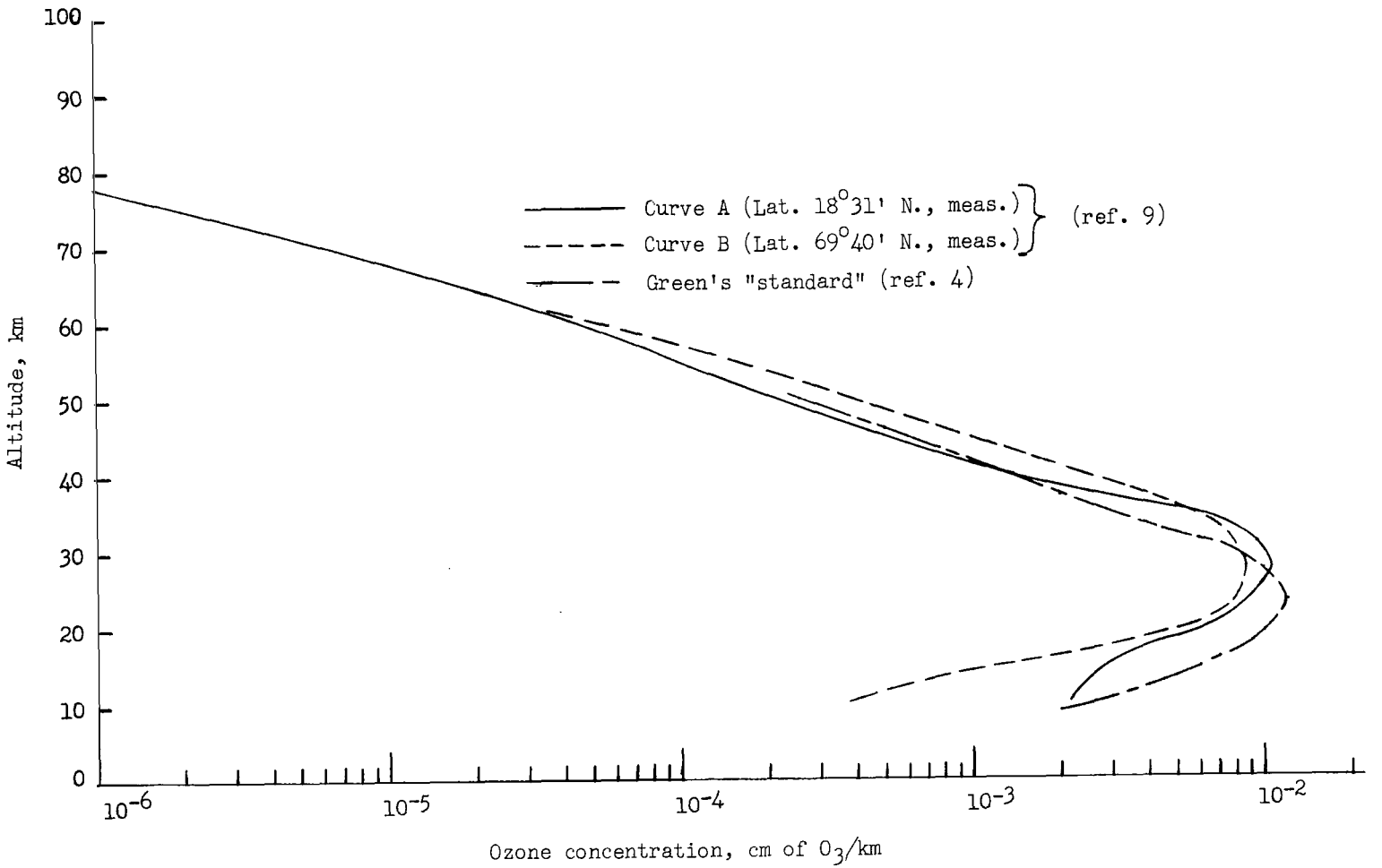

Figure 7.- Ozone distribution.

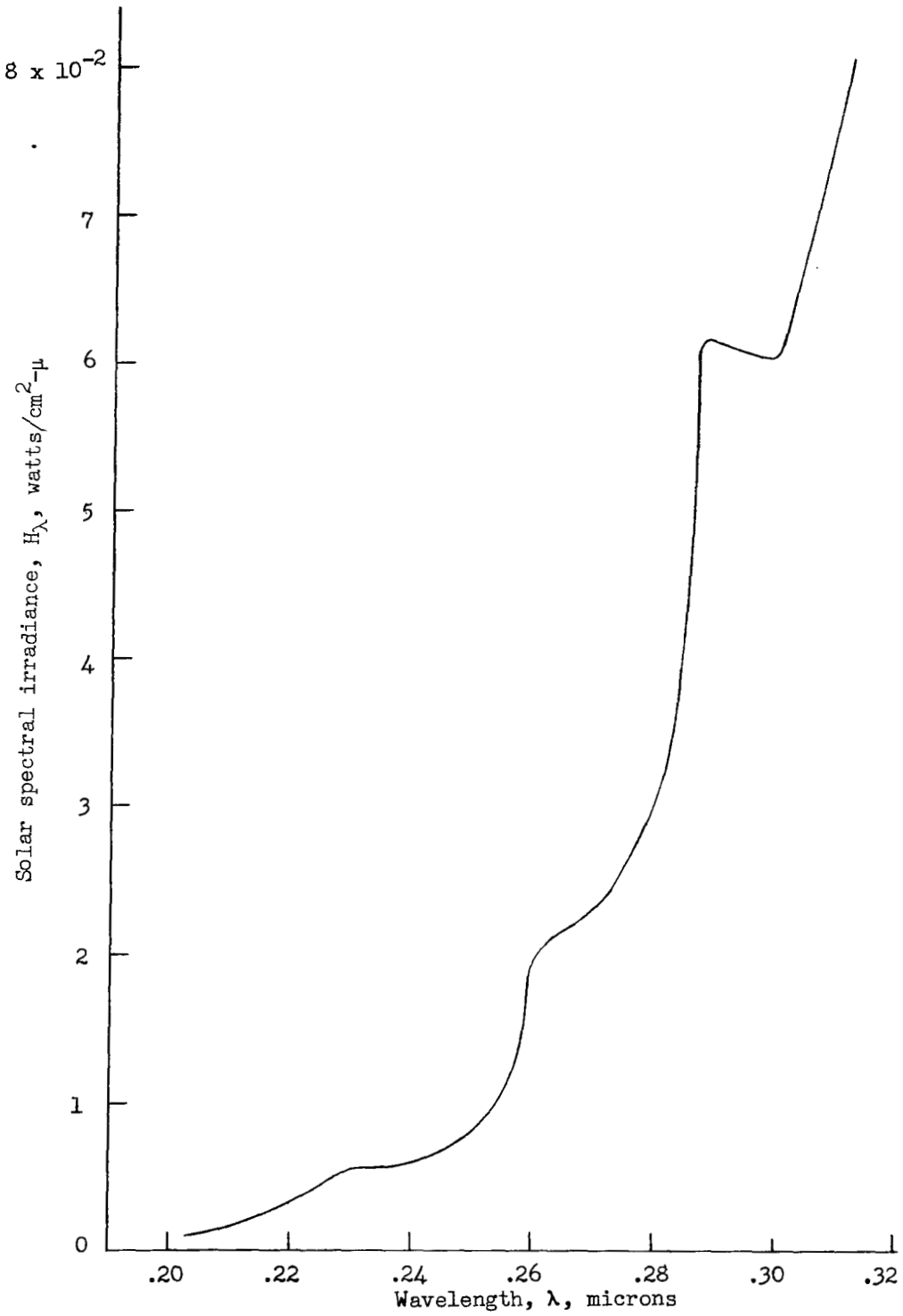

Figure 8.- Solar spectral irradiance.

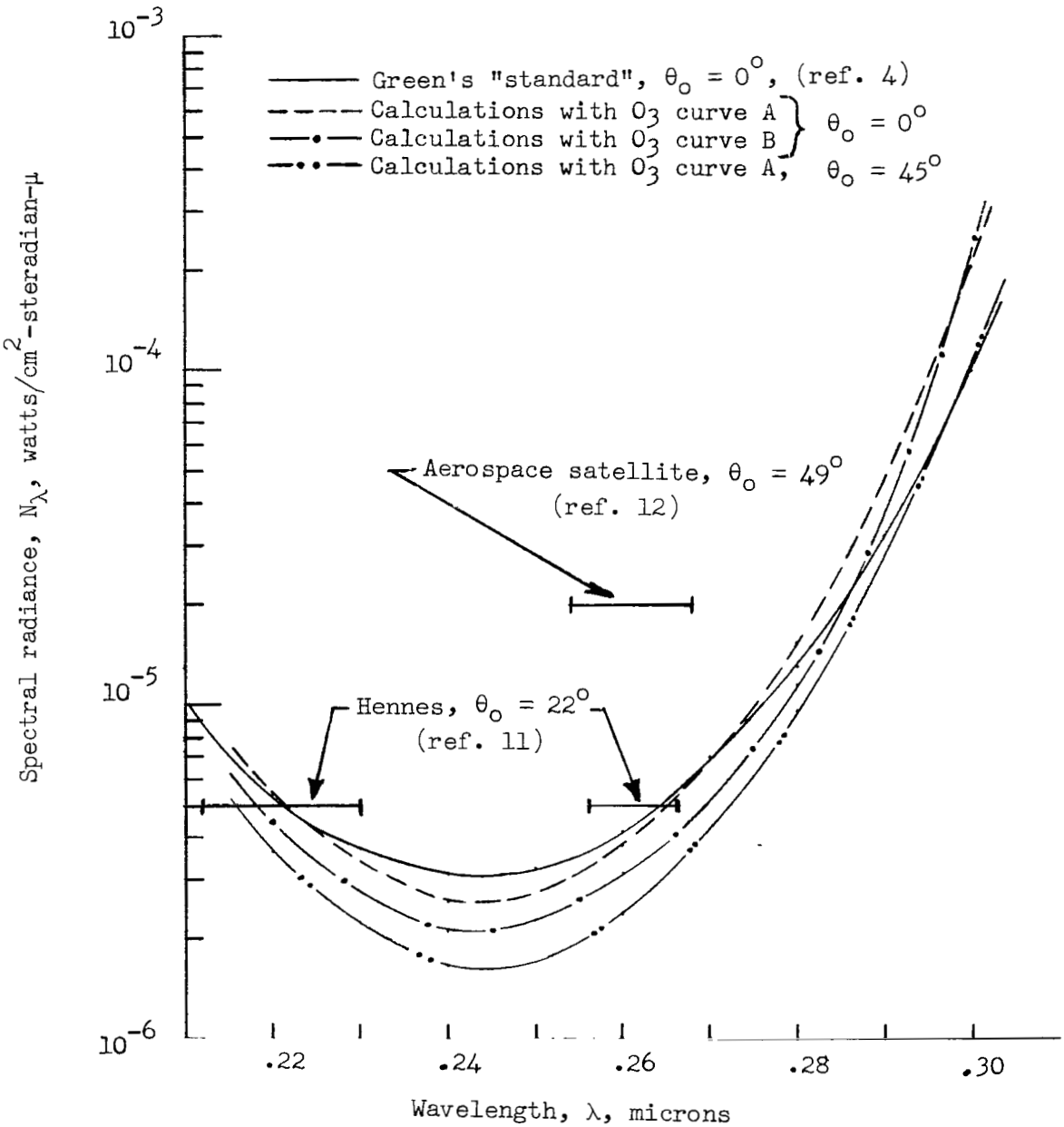

Figure 9.- Nadir radiance for middle ultraviolet wavelengths.

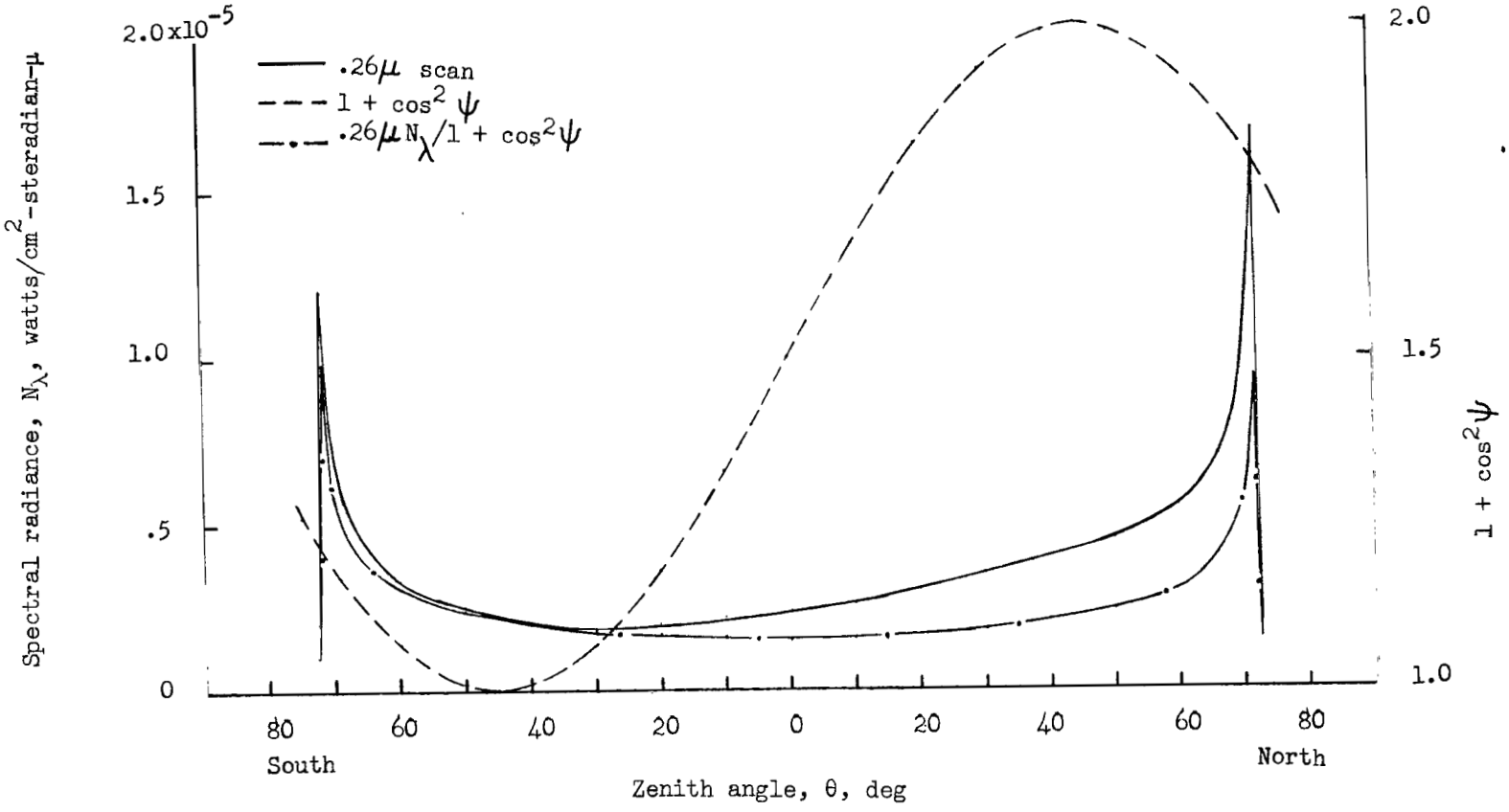

Figure 10.- The 0.26μ scan and its ψ-effect for $\theta_o = 45^o$, $\phi_o = 180^o$.

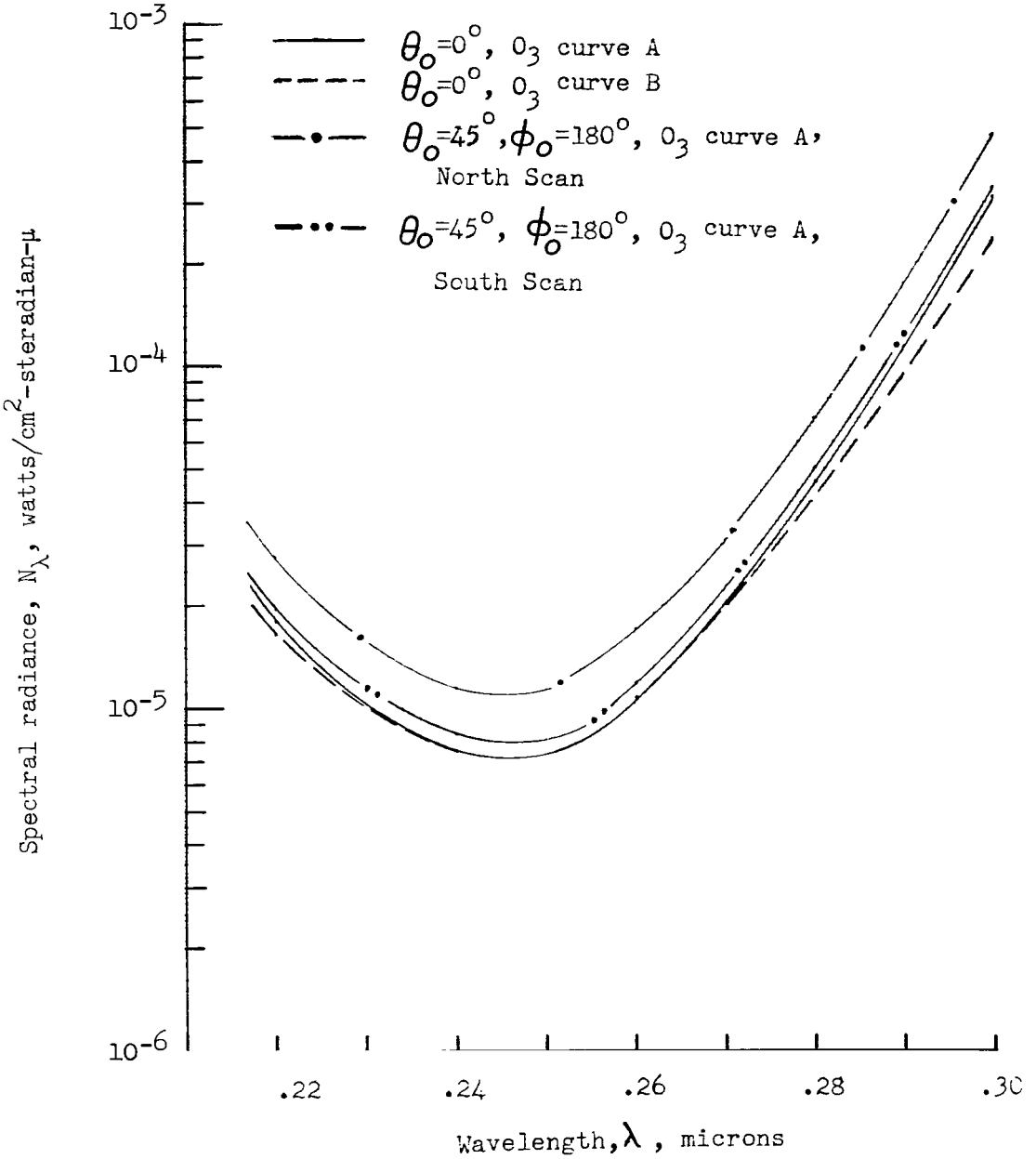

Figure 11.- Spectral radiances of the peaks for various wavelengths.

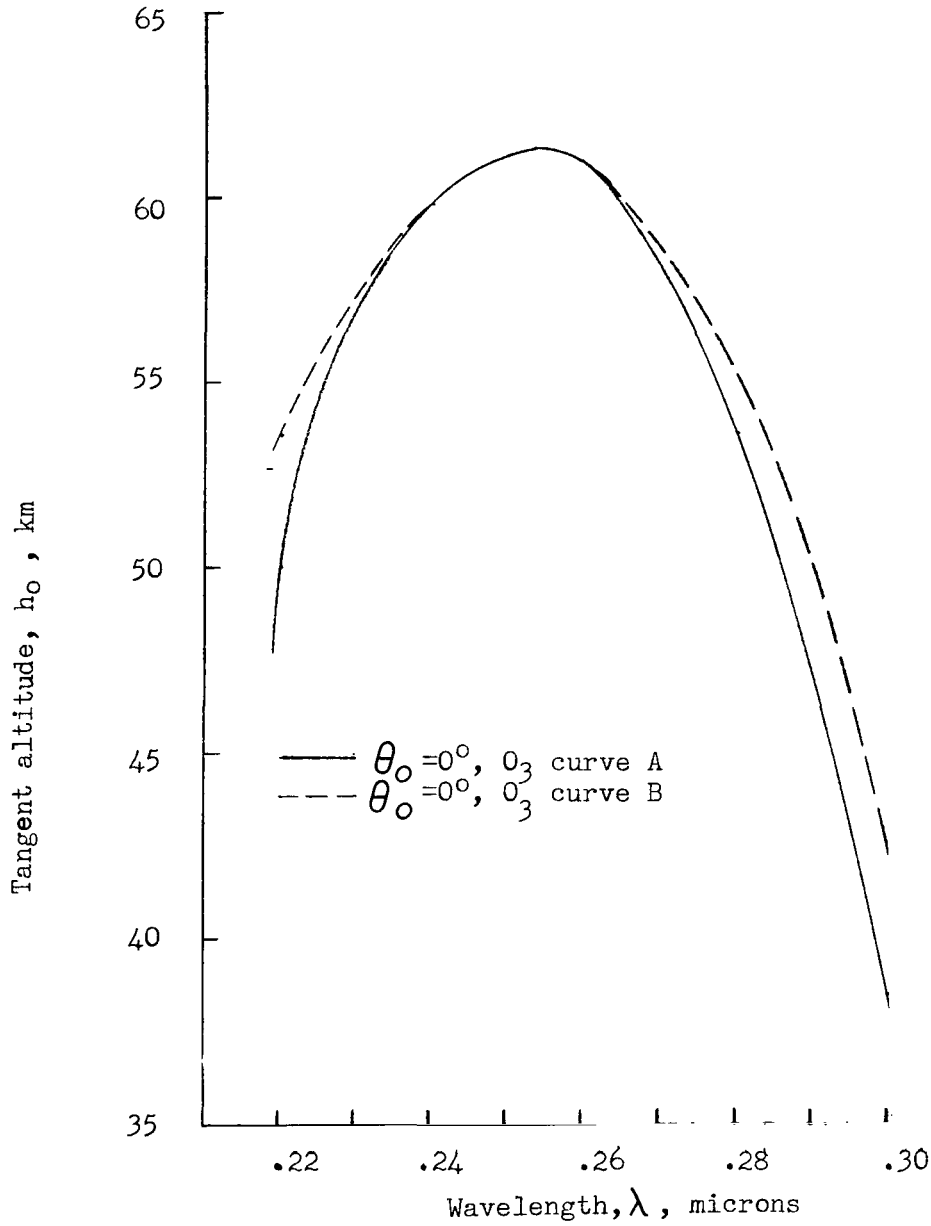

Figure 12.- Tangent altitude of peaks as a function of wavelength for different ozone distributions.

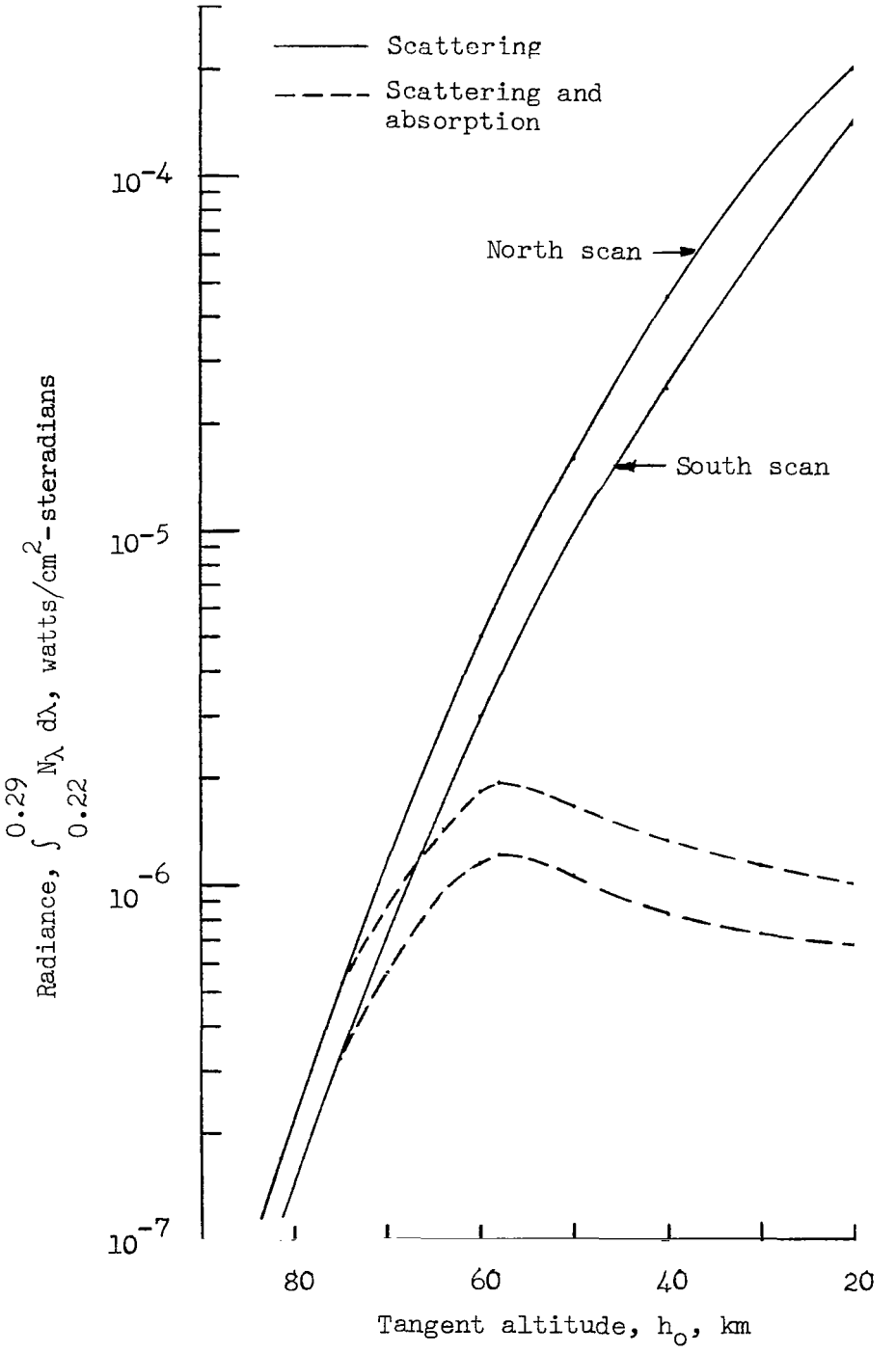

Figure 13.- Integrated radiance, 0.22μ to 0.29μ, of the limb for scattering and for scattering and absorption. ϕ_o = 171.19°; θ_o = 57.15°; h = 450 km.

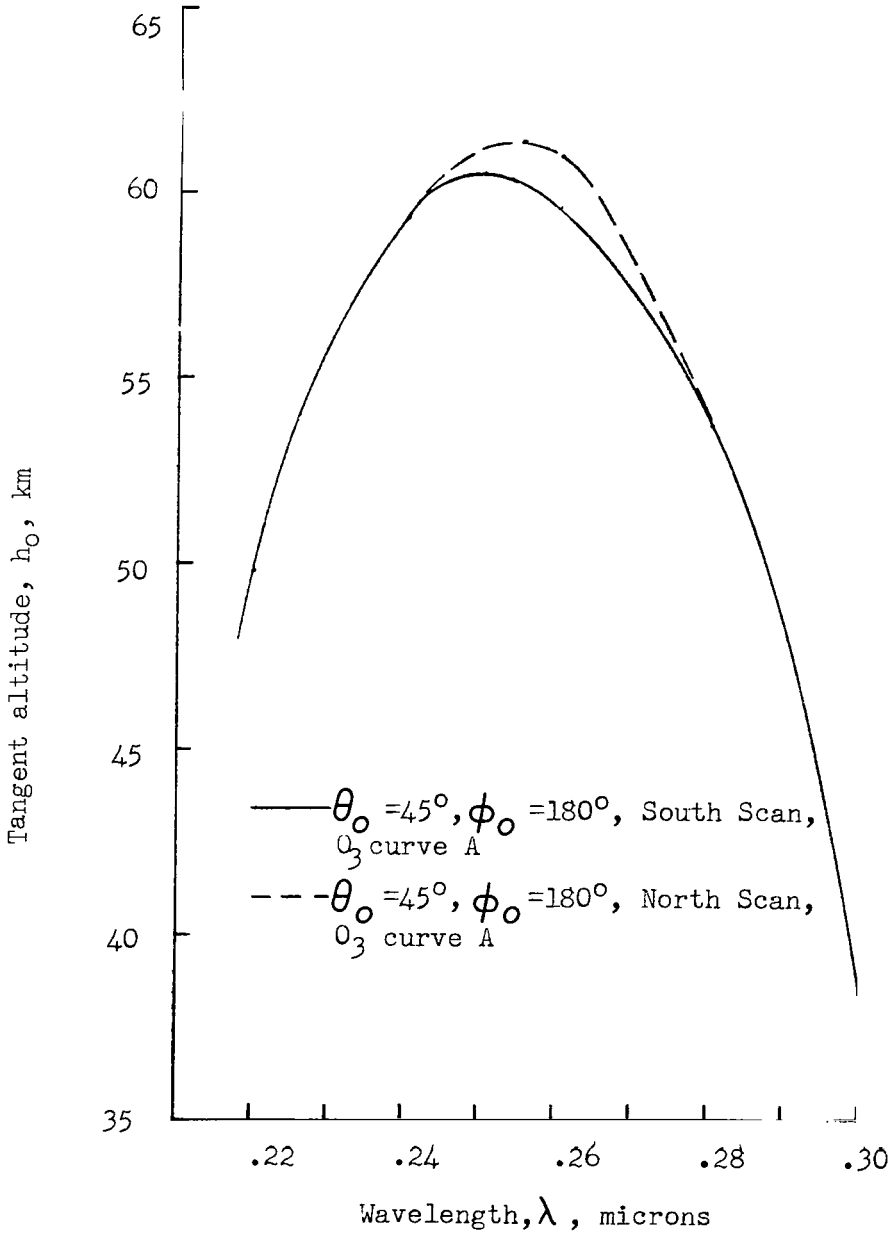

Figure 14.- Tangent altitude of peaks for various wavelengths.

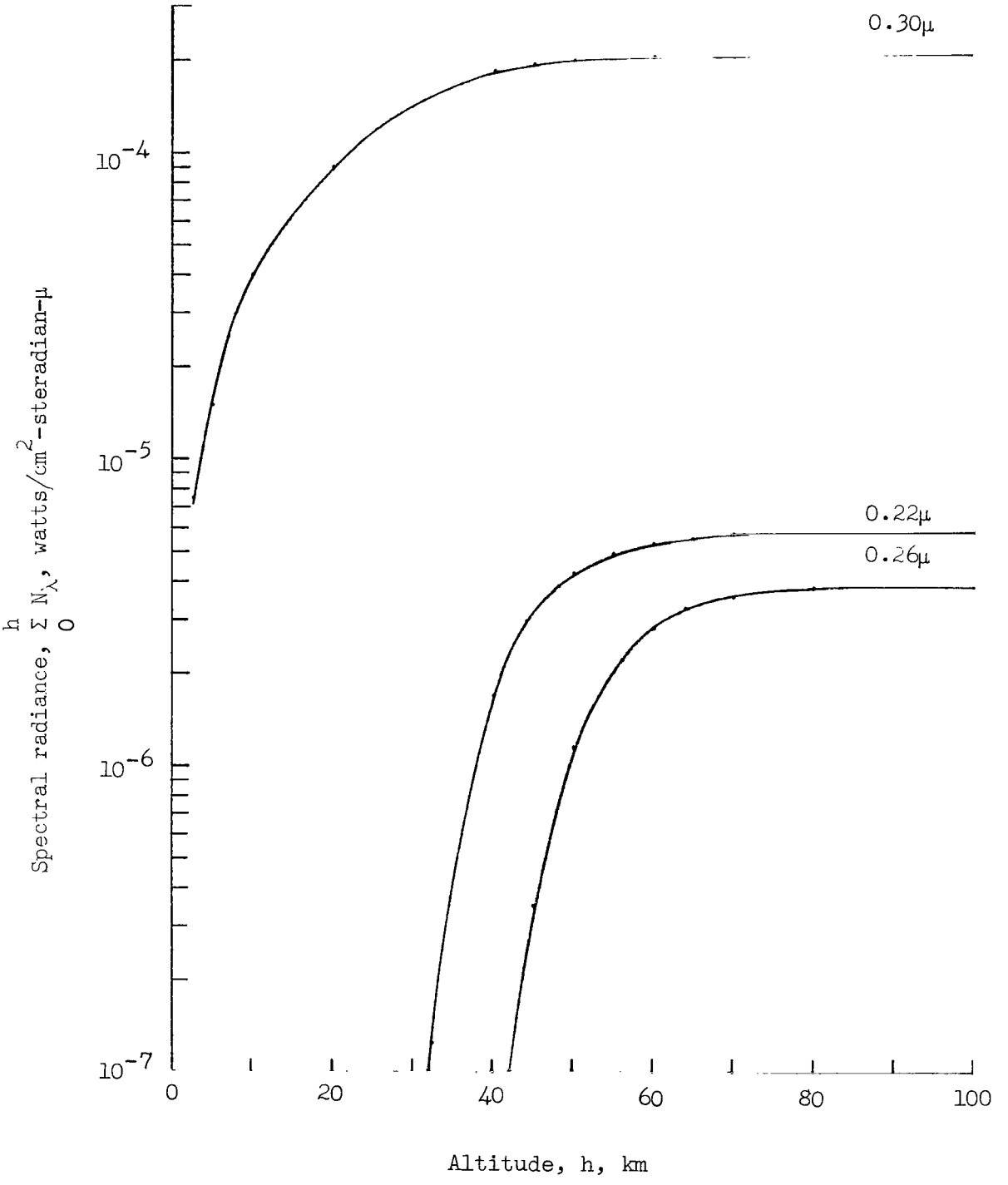

Figure 15.- The contribution from different altitudes to the total emerging radiance at various wavelengths using O_3 curve A for the nadir.

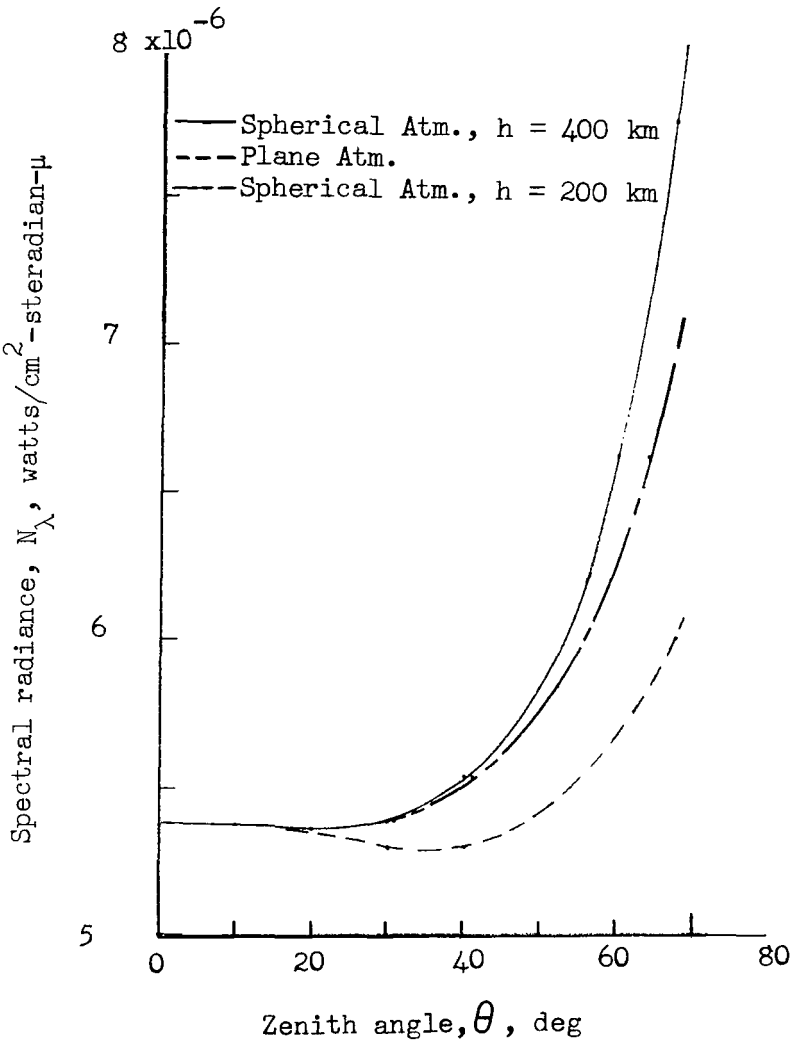

Figure 16.- Comparison of the 0.26μ spectral radiances from the plane-parallel and spherical atmospheres for $\theta_o = 0^o$ and using Green's O_3 distribution.

"The aeronautical and space activities of the United States shall be conducted so as to contribute . . . to the expansion of human knowledge of phenomena in the atmosphere and space. The Administration shall provide for the widest practicable and appropriate dissemination of information concerning its activities and the results thereof."

—NATIONAL AERONAUTICS AND SPACE ACT OF 1958

NASA SCIENTIFIC AND TECHNICAL PUBLICATIONS

TECHNICAL REPORTS: Scientific and technical information considered important, complete, and a lasting contribution to existing knowledge.

TECHNICAL NOTES: Information less broad in scope but nevertheless of importance as a contribution to existing knowledge.

TECHNICAL MEMORANDUMS: Information receiving limited distribution because of preliminary data, security classification, or other reasons.

CONTRACTOR REPORTS: Technical information generated in connection with a NASA contract or grant and released under NASA auspices.

TECHNICAL TRANSLATIONS: Information published in a foreign language considered to merit NASA distribution in English.

TECHNICAL REPRINTS: Information derived from NASA activities and initially published in the form of journal articles.

SPECIAL PUBLICATIONS: Information derived from or of value to NASA activities but not necessarily reporting the results of individual NASA-programmed scientific efforts. Publications include conference proceedings, monographs, data compilations, handbooks, sourcebooks, and special bibliographies.

Details on the availability of these publications may be obtained from:

SCIENTIFIC AND TECHNICAL INFORMATION DIVISION

NATIONAL AERONAUTICS AND SPACE ADMINISTRATION

Washington, D.C. 20546